First Experimental Limit on the $^{19}Ne(p,\gamma)^{20}Na$ Resonance Strength, of Astrophysical Interest

R. D. Page,[1] G. Vancraeynest,[2] A. C. Shotter,[1] M. Huyse,[2] C. R. Bain,[1] F. Binon,[3] R. Coszach,[4] T. Davinson,[1] P. Decrock,[2] Th. Delbar,[4] P. Duhamel,[3] M. Gaelens,[2] W. Galster,[4] P. Leleux,[4] I. Licot,[4,*] E. Lienard,[4] P. Lipnik,[4] C. Michotte,[4] A. Ninane,[4] P. J. Sellin,[1,†] Cs. Sükösd,[5] P. Van Duppen,[2,‡] J. Vanhorenbeeck,[3] J. Vervier,[4] M. Wiescher,[6] and P. J. Woods[1]

[1]*Department of Physics and Astronomy, University of Edinburgh, The King's Buildings, Edinburgh EH9 3JZ, United Kingdom*
[2]*Instituut voor Kern-en Stralingsfysika, Katholieke Universiteit Leuven, Leuven, B-3001 Belgium*
[3]*Institut d'Astronomie, d'Astrophysique et de Géophysique, Université Libre de Bruxelles, B-1050 Bruxelles, Belgium*
[4]*Institut de Physique Nucléaire, Université Catholique de Louvain, Louvain-la-Neuve, B-1348 Belgium*
[5]*Institute of Nuclear Techniques, Technical University of Budapest, H-1521 Budapest, Hungary*
[6]*Department of Physics, University of Notre Dame, Notre Dame, Indiana 46556*

(Received 18 August 1994)

The $^{19}Ne(p,\gamma)^{20}Na$ reaction may influence considerably the reaction flow between the CNO and NeNa mass regions in high temperature hydrogen burning conditions. The 447 keV resonance has been studied by exploiting radioactive ^{19}Ne beams with novel detection techniques to measure β^+-delayed α radioactivity of ^{20}Na nuclei produced in reactions with polyethylene targets. A 90% C.L. upper limit of 18 meV for the resonance strength has been determined and implications for the spin assignment of the 2.646 MeV state in ^{20}Na and the stellar reaction rate are discussed.

PACS numbers: 25.40.Lw, 25.60.+v, 27.30.+t, 95.30.Cq

Energy production and nucleosynthesis in hot and explosive stellar hydrogen burning are characterized by the hot CNO cycles [1] and the *rp* process [2]. It has been suggested that at high temperatures the CNO cycles and *rp* process are linked by the capture reaction sequence $^{15}O(\alpha,\gamma)^{19}Ne(p,\gamma)^{20}Na$, with higher mass nuclides being synthesized from the initial C, N, O material. The reaction flow depends critically on the reaction rates of both capture processes, with the weaker reaction determining the breakout conditions [3]. However, both rates are sufficiently uncertain that the actual temperature and density conditions for breakout are still ill defined.

It has been proposed [4–7] that the reaction rate for $^{19}Ne(p,\gamma)^{20}Na$ is determined by a low energy resonance at 447 keV. The corresponding level in ^{20}Na at 2.646 MeV has been observed in both $^{20}Ne(p,n)^{20}Na$ [5] and $^{19}Ne(^3He,t)^{20}Na$ [4–7]. On the basis of angular distribution measurements and the known level sequence of the mirror nucleus ^{20}F, a $J^\pi = 1^+$ assignment has been suggested for this state. This level, however, was not observed in β-delayed proton decays of ^{20}Mg, which predominantly proceed via $J^\pi = 1^+$ states in ^{20}Na [8–10]. This is consistent with the proposed intruder character [11] of the suggested mirror state at 3.173 MeV in ^{20}F [6]. The $^{19}Ne(p,\gamma)^{20}Na$ resonance strength of $\omega\gamma = 6$ meV predicted for this 1^+ assignment is mainly determined by the partial γ width, estimated to be $\Gamma_\gamma = 9$ meV [6].

This mirror assignment has been questioned by Brown *et al.* [12] who identify the 2.646 MeV level in ^{20}Na with the $J^\pi = 3^+$ level at 2.966 MeV in ^{20}F. This assignment is based on Coulomb shift calculations and a comparison of the $^{20}Ne(^3He,t)$ and $(t,^3He)$ reactions [13]. Shell model calculations of the single particle and γ strength of this 3^+ state in ^{20}Na lead to a considerably larger resonance strength of $\omega\gamma = 80$ meV, mainly due to a higher γ width, $\Gamma_\gamma = 120$ meV, than anticipated for the 1^+ assignment.

The advent of radioactive beams has created new opportunities to measure the $^{19}Ne(p,\gamma)^{20}Na$ reaction rate experimentally. Most experiments to date [8–10] have investigated the β^+-delayed proton decays of ^{20}Mg nuclei produced in intermediate energy reactions, but all have failed to identify protons emitted from the 2.646 MeV level. However, the availability of intense beams of ^{19}Ne ions at the Louvain-la-Neuve radioactive beam facility [14] affords the possibility of a direct measurement [15]. Although the low estimated yield would preclude direct detection of the capture γ rays, a measurement is feasible by detecting the subsequent radioactive decays of the ^{20}Na nuclei (half-life = 448 ms) produced in the reaction. The dominant decay branch of ^{20}Na is β^+ decay to the 2^+ state at 1.63 MeV in ^{20}Ne but ~20% of the β^+-decay strength feeds higher lying levels which promptly decay by α-particle emission. Two novel techniques have been developed to determine the $^{19}Ne(p,\gamma)^{20}Na$ reaction rate by measuring the yield of these β^+-delayed α lines, the absolute branching ratios of which are known [16].

The key problem to be overcome is detecting the anticipated small yield of these low energy β^+-delayed α particles in the presence of an intense background, arising mainly from radioactivity of the unreacted ^{19}Ne beam ($\sim 5 \times 10^8$ β^+ decays s^{-1}). In the first technique this problem is solved by employing double-sided silicon strip detectors (DSSSDs) [15] while the second method

 0031-9007/94/73(23)/3066(4)$06.00

uses polycarbonate solid state nuclear track detectors (SSNTDs) which are etched electrochemically [17].

DSSSDs have previously been used to study proton radioactivity and have been shown to be highly insensitive to β particles [18]. The DSSSDs comprise 48 300 μm $\times$ 16 mm strips on each face, with the two sets of strips orthogonally crossed. Each strip overlap defines a pixel which, for the 34 and 67 μm thick DSSSDs used in the present experiment, represents a very small volume of silicon compared with typical β-particle ranges. The insensitivity of DSSSDs to β particles is thus a direct consequence of this high degree of segmentation.

A polyethylene (PE) or deuterated PE target foil mounted on a wheel is irradiated by a well-collimated ^{19}Ne beam. ^{20}Na nuclei produced by the reaction recoil out of the target and are implanted along with unreacted ^{19}Ne ions into a stopping surface which is mounted so that the ions are incident at a grazing angle of 12.5°. This reduces the depth at which the ^{20}Na ions are implanted by more than a factor of 4 compared with perpendicular implantation. This is important because deep implantation would result in a large energy loss for the emitted β^+-delayed α particles so that clean separation from a β^+ tail arising from decays of the beam species is not achieved. Furthermore, straggling and angle of emission effects dramatically broaden the α lines for increasing implantation depths, whereas peaks should be as narrow as possible when searching for weak signals.

The stopping surface is a 2 μm thick layer of aluminum evaporated onto a 5 cm $\times$ 3 cm optical quality glass slide. Two slides are mounted on opposite sides of a square perspex disk which is rotated through 180° every 870 ms, bringing the recently irradiated surface in front of two adjacent DSSSDs. The corners of the disk are cut away to allow the DSSSDs to be stationed 11 mm from the stopping surface. This close geometry ensures a large solid angle (11.5%) for efficient β^+-delayed α-particle detection. The rotation takes 127 ms, so 36% of ^{20}Na nuclei implanted into the surfaces decay in front of the DSSSDs, giving an overall ^{20}Na detection efficiency of 0.5%.

In the SSNTD technique, ^{20}Na ions produced in the PE target are slowed down using an aluminum degrader foil and implanted normally into a 1.5 mg cm^{-2} thick aluminum stopper foil mounted on one arm of a "windmill." The degrader foil thickness is chosen to implant ^{20}Na ions in the middle of the stopper foil. The windmill has four such arms: while one stopper foil is in the collection position, the remaining three are sandwiched between pairs of SSNTD foils, mounted 2 mm apart. The windmill is rotated through 90° every 1030 ms, with the rotation taking 110 ms, so 30.6% of the produced ^{20}Na activity decays between the first detector pair. β^+-delayed α particles can escape through either surface of the stopper foil and cause radiation damage when they penetrate into the SSNTD material. When the SSNTDs are subsequently etched electrochemically, treelike structures develop where the α particles penetrated, and these are large enough to be counted using an optical microscope or microfiche reader [17]. The three successive detection stations provide a clear lifetime signature.

The SSNTD α-particle detection efficiency was determined as a function of energy and angle of incidence using beams of Rutherford backscattered α particles. Together with results from [17], the sensitive energy window for normal incidence was determined to be 0.3–2.0 MeV, indicating that only the 2.15 MeV β^+-delayed α particles, slowed down as they emerged from the stopper foil, would be registered by the SSNTDs. The mean ^{20}Na implantation depth and the energy as a function of the angle of emergence of α particles from the stopper foil were determined [19] and convolution of the latter with the detection efficiency function yielded an effective detection efficiency of (35 $\pm$ 4)%. Hence the overall efficiency of the SSNTD method is 1.7%. The background level of tracks inherent to the SSNTDs ($\sim$20 cm^{-2}) was reduced to 1.56 $\pm$ 0.09 cm^{-2} by heating them for three days at 390 K under atmospheric pressure and by careful analysis of the etched hole shapes. In the experiment, part of each SSNTD foil was shielded: Determining the track density in this 3.7 cm^2 shielded region provided a further check on the intrinsic background level. The insensitivity of the SSNTDs to β particles was demonstrated by irradiations with β sources up to doses of 2 $\times$ 10^4 Gy and by control SSNTDs in the reaction chamber during the experiment. Polycarbonate is also insensitive to protons when etched electrochemically as they do not cause significant radiation damage [19,20].

Both techniques determine the integrated beam current by using silicon detectors to measure the yields of scattered beam particles and recoiling protons, deuterons and carbon ions knocked out of the target by the 11.4 MeV ^{19}Ne beam. Determining the proton (or deuteron) and carbon yield relative to that of the β^+ radioactivity of the beam allows the target thickness and stoichiometry during the course of the experiment to be monitored and corrected for on a run by run basis [21]. The DSSSDs and SSNTDs were carefully shielded to prevent background arising from scattered beam particles.

Initially both methods were used to investigate the ^{19}Ne$(d,n)^{20}$Na reaction, which has an expected rate several orders of magnitude higher than that of the ^{19}Ne$(p,\gamma)^{20}$Na reaction. This provided an opportunity to prove the viability of each method and to check their mutual consistency. It was also important because the ^{19}Ne$(d,n)^{20}$Na reaction may provide a significant contribution to any observed ^{20}Na production rate when studying the ^{19}Ne$(p,\gamma)^{20}$Na reaction, even though natural hydrogen comprises only 0.015% deuterium [15].

Using the DSSSD method, the cross section for the ^{19}Ne$(d,n)^{20}$Na reaction was measured by bombarding 180 and 60 μg cm^{-2} thick deuterated PE targets with 14–28

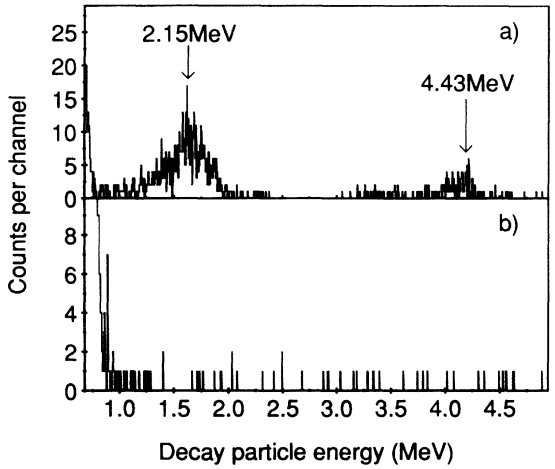

FIG. 1. Energy spectrum of events observed in the DSSSDs using an 11.4 MeV beam of ^{19}Ne ions to bombard (a) a deuterated PE target and (b) a PE target. The two principal ^{20}Na β^+-delayed α-decay lines with energies of 2.15 and 4.43 MeV are indicated in (a). At the low energy end of these spectra is the tail due to β^+ radioactivity of the unreacted ^{19}Ne ions, which are also implanted into the stopping surface. This is more intense in (b) reflecting the total dose of 1.2×10^{14} ^{19}Ne ions, compared with 8.4×10^{12} ^{19}Ne ions in (a).

particle-pA (ppA) beams of ^{19}Ne ions for periods of 12.9 and 6.2 h, respectively. Figure 1(a) shows the combined energy spectrum for these data. The two main $\beta+$-delayed α-decay lines at 2.15 and 4.43 MeV are clearly visible, shifted down in energy because of energy losses in the stopping surface.

In the SSNTD method a 250 μg cm^{-2} thick deuterated PE foil was irradiated with a 34 ppA ^{19}Ne beam.

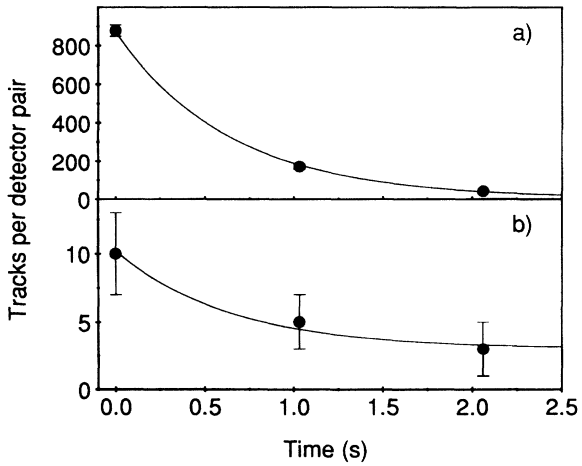

FIG. 2. Observed number of tracks at the successive detector positions in (a) the ^{19}Ne$(d,n)^{20}$Na run (dose = 2.3×10^{12} ^{19}Ne ions) and (b) the ^{19}Ne$(p,\gamma)^{20}$Na runs (dose= 6.7×10^{13} ^{19}Ne ions). The solid lines are fits of the initial activity and a constant background to the data assuming the ^{20}Na half-life.

Figure 2(a) shows the number of tracks counted at the three detector positions. The initial activity and a constant background were fitted to the data assuming the ^{20}Na half-life. The fitted background value agrees well with the average intrinsic background level after annealing. The average hydrogen to carbon ratios of the targets were 1.7 and 1.8 for the SSNTD and DSSSD measurements, respectively, with 96% of the hydrogen being deuterium.

From the yield of β^+-delayed α particles the cross section for the ^{19}Ne$(d,n)^{20}$Na reaction was independently determined as 1.4 $\pm$ 0.2 mb by both methods, proving their mutual consistency. In the ^{19}Ne$(p,\gamma)^{20}$Na reaction rate measurement, the ^{19}Ne$(d,n)^{20}$Na reaction cross section would correspond to a false "resonance strength" of $\sim$4 meV in either method, so this effect was taken into account in the ^{19}Ne$(p,\gamma)^{20}$Na data analysis.

In the ^{19}Ne$(p,\gamma)^{20}$Na reaction rate measurement, the DSSSD method used $\sim$90 ppA beams of ^{19}Ne ions to irradiate 225–250 μg cm^{-2} thick PE targets (average hydrogen to carbon ratio = 0.99). The resulting energy spectrum is shown in Fig. 1(b). There is no clear evidence for the characteristic ^{20}Na $\beta+$-delayed α-decay lines but rather there appears to be a fairly constant background, which extends up to $\sim$8 MeV. Extensive background measurements, both online and offline, have failed to reproduce this background or to elucidate its origin. Nevertheless, this spectrum was analyzed in order to determine an upper limit on the yield of β^+-delayed α particles.

The 2.15 MeV β^+-delayed α-decay line produced with a PE target was calculated to be very close in shape and energy to that actually measured for the deuterated PE target. Because of the low energy tail on the α line, the region within $\pm$0.5 FWHM ($\pm$180 keV) of the 2.15 MeV peak centroid was analyzed, rather than the whole peak. The proportion of counts in the 2.15 MeV peak appearing in this region was determined from the spectrum of Fig. 1(a) as (60 $\pm$ 4)%. There are 4 events in the corresponding region of Fig. 1(b), compared with a total background of 4.8 $\pm$ 0.3 counts estimated from an extrapolation of the background from higher energies and the yield expected from reactions of the natural deuterium content of the target. The monitor detector proton yields indicate a resonance strength of 4.6 $\pm$ 1.2 meV per count in the region of interest arising from the ^{19}Ne$(p,\gamma)^{20}$Na reaction. From this a 90% confidence level upper limit of 21 meV was determined for the 447 keV resonance strength [22].

In the SSNTD technique 170 μg cm^{-2} thick PE targets were irradiated with 25–85 ppA ^{19}Ne beams and had an average hydrogen to carbon ratio of 0.77. One set of six SSNTDs was used throughout and track counting was restricted to the region in which the tracks had appeared in the ^{19}Ne$(d,n)^{20}$Na experiment (1.9 cm^2 per SSNTD pair), in order to minimize the intrinsic background contribution. Figure 2(b) shows the observed number of tracks on

the successive detector pairs. A maximum likelihood fit yielded an initial activity with the ^{20}Na half-life of $7.2^{+4.2}_{-3.7}$ tracks on the first detector pair and a background of $3.0^{+1.9}_{-1.3}$ tracks per SSNTD pair, in good agreement with the expected average background. The ^{19}Ne$(d,n)^{20}$Na reaction contribution corresponds to 2.1 ± 0.2 tracks on the first pair of SSNTDs, and a conversion of 2.4 ± 0.6 meV per track at the first detection position was deduced from the monitor detector proton yields. The number of tracks with a ^{20}Na lifetime corrected for the ^{19}Ne$(d,n)^{20}$Na contribution is $5.1^{+4.4}_{-4.0}$, which would correspond to a resonance strength of $\omega\gamma = 12^{+11}_{-10}$ meV. However, this measurement is at the limit of the technique's sensitivity and the possibility of a contribution from an unknown background activity cannot be excluded. Therefore only an analysis in terms of upper limits was performed, giving a 90% confidence level upper limit of 26 meV for the strength of the 447 keV resonance [22].

A 90% confidence level upper limit of $\omega\gamma \leq 18$ meV was deduced from the combined results of the two methods [22]. This is consistent with the resonance strength of $\omega\gamma = 6$ meV predicted by Lamm *et al.* [6], based on a $J^\pi = 1^+$ intruder state assignment, although it does not exclude the possibility of a much smaller resonance strength arising because of a lower γ width. However, the limit is significantly lower than the value of 80 meV estimated by Brown *et al.* [12], based on the $J^\pi = 3^+$ assignment for the resonance. Furthermore, from the recently observed upper limit of $\tau \leq 15$ fs (90% confidence level) for the lifetime of the proposed analog 3^+ state in ^{20}F at 2.966 MeV [23] and adopting the proton widths from Ref. [12], a 90% confidence level lower limit of 20 meV is deduced for the strength of a 3^+ resonance. Comparison of this lower limit with the 90% confidence level upper limit of 18 meV, obtained by combining the results of the present measurements, indicates that a $J^\pi = 3^+$ assignment for the state at 2.646 MeV in ^{20}Na would be excluded with 99% confidence. However, a lower 3^+ resonance strength could be expected if the ratio of proton widths to the ground state and first excited state in ^{19}Ne is significantly smaller than calculated [12].

The present work provides the first experimental limit on the resonance strength of the 2.646 MeV level and indicates that the reaction rate is significantly lower than was recently suggested [12]. To evaluate fully the influence of the ^{19}Ne$(p,\gamma)^{20}$Na reaction on breakout from the CNO cycles into the *rp* process, a lower limit on the resonance strength of the 2.646 MeV level has to be obtained, together with measurements of γ widths of higher lying levels and the direct capture process. An experimental study of higher lying levels is currently in progress, but a lower limit on the 2.646 MeV level resonance strength will require significant advances in sensitivity and the ^{19}Ne beam intensity.

The authors would like to thank staff at Louvain-la-Neuve for technical assistance, Joachim Görres for many useful discussions, and H. Vanmarcke and P. Willeborts for etching the SSNTDs at the SCK, Mol, Belgium. F. B., P. Leleax, and J. Vaahorenbeeck are Senior Research Associates and G. V. is a Research Assistant of the NFWO/FNRS, Belgium; M. G. is a fellow of the Belgian IWONL. This work presents research results of the Belgian Programme on Interuniversity Poles of Attraction initiated by the Belgian state, Federal Services of Scientific, Technical and Cultural Affairs and was also supported by the UK SERC.

*Present address: University of Sao Paolo, Sao Paulo, Brazil.

†Present address: Department of Physics, University of Sheffield, Sheffield, S3 7RH, United Kingdom.

‡Present address: CERN, PPE-Division, CH-1211 Geneva 23, Switzerland.

[1] J. Audouze *et al.*, Astrophys. J. **184**, 493 (1973).
[2] R. K. Wallace and S. E. Woosley, Astrophys. J. Suppl. **45**, 389 (1981).
[3] L. VanWormer *et al.* (to be published).
[4] M. Wiescher *et al.*, Lecture Notes in Physics **287**, 54 (1987).
[5] S. Kubono *et al.*, Z. Phys. A **334**, 511 (1989).
[6] L. O. Lamm *et al.*, Nucl. Phys. **A510**, 503 (1990).
[7] M. S. Smith *et al.*, Nucl. Phys. **A536**, 333 (1992).
[8] S. Kubono *et al.*, Phys. Rev. C **46**, 361 (1992).
[9] J. Görres *et al.*, Phys. Rev. C **46**, R833 (1992).
[10] A. Piechaczek *et al.*, in *Proceedings of the Third International Conference on Radioactive Nuclear Beams, Lansing, Michigan, 1993*, edited by D. J. Morrissey (Editions Frontières, Gif-sur-Yvette, France, 1993), p. 495.
[11] R. Medoff *et al.*, Phys. Rev. C **14**, 1 (1976).
[12] B. A. Brown *et al.*, Phys. Rev. C **48**, 1456 (1993).
[13] N. M. Clarke *et al.*, J. Phys. G **16**, 1547 (1990).
[14] D. Darquennes *et al.*, Phys. Rev. C **42**, R804 (1990).
[15] R. D. Page *et al.*, in *Proceedings of the Third International Conference on Radioactive Nuclear Beams, Lansing, Michigan, 1993,* edited by D. J. Morrissey (Editions Frontières, Gif-sur-Yvette, France, 1993), p. 489.
[16] E. T. H. Clifford *et al.*, Nucl. Phys. **A493**, 293 (1989).
[17] H. Vanmarcke *et al.*, Nucl. Tracks **12**, 689 (1986).
[18] P. J. Sellin *et al.*, Nucl. Instrum. Methods Phys. Res., Sect. A **311**, 217 (1992).
[19] L. C. Northcliffe and R. F. Schilling, At. Nucl. Data Tables **A7**, 233 (1970).
[20] S. A. Durrani and R. K. Bull, *Solid State Nuclear Track Detection* (Pergamon Press, New York, 1986), p. 181.
[21] W. Galster *et al.*, Phys. Rev. C **44**, 2776 (1991).
[22] Particle Data Group, Phys. Lett. **B239**, III.34 (1990).
[23] J. Görres *et al.*, Phys. Rev. C **50**, R1270 (1994).